ARMY RESEARCH LABORATORY

A Nonlinear Model Predictive Observer for Smart Projectile Applications

by Mark Costello and Ryan Letniak

ARL-CR-0603 **March 2008**

prepared by

Georgia Institute of Technology
Atlanta, Georgia

and

American Institute of Aeronautics and Astronautics
Reston, Virginia

under contract

W911QX-06-C-0113

NOTICES

Disclaimers

The findings in this report are not to be construed as an official Department of the Army position unless so designated by other authorized documents.

Citation of manufacturer's or trade names does not constitute an official endorsement or approval of the use thereof.

DESTRUCTION NOTICE—Destroy this report when it is no longer needed. Do not return it to the originator.

Army Research Laboratory
Aberdeen Proving Ground, MD 21005-5069

ARL-CR-0603 **March 2008**

A Nonlinear Model Predictive Observer for Smart Projectile Applications

Mark Costello
School of Aerospace Engineering, Georgia Institute of Technology

Ryan Letniak
American Institute of Aeronautics and Astronautics

prepared by

Georgia Institute of Technology
Atlanta, Georgia

and

American Institute of Aeronautics and Astronautics
Reston, Virginia

under contract

W911QX-06-C-0113

REPORT DOCUMENTATION PAGE

Form Approved
OMB No. 0704-0188

1. REPORT DATE *(DD-MM-YYYY)*	2. REPORT TYPE	3. DATES COVERED (From - To)
March 2008	Final	October 2006 to September 2007

4. TITLE AND SUBTITLE

A Nonlinear Model Predictive Observer for Smart Projectile Applications

5a. CONTRACT NUMBER
W911QX-06-C-0113

5b. GRANT NUMBER

5c. PROGRAM ELEMENT NUMBER

6. AUTHOR(S)

Mark Costello (GIT); Ryan Letniak (AIAA)

5d. PROJECT NUMBER
AH80

5e. TASK NUMBER

5f. WORK UNIT NUMBER

7. PERFORMING ORGANIZATION NAME(S) AND ADDRESS(ES)

Georgia Institute of Technology
Atlanta, Georgia

American Institute of Aeronautics and Astronautics
Reston, Virginia

8. PERFORMING ORGANIZATION REPORT NUMBER
ARL-CR-0603

9. SPONSORING/MONITORING AGENCY NAME(S) AND ADDRESS(ES)

U.S. Army Research Laboratory
Weapons and Materials Research Directorate
Aberdeen Proving Ground, MD 21005-5069

10. SPONSOR/MONITOR'S ACRONYM(S)

11. SPONSOR/MONITOR'S REPORT NUMBER(S)

12. DISTRIBUTION/AVAILABILITY STATEMENT

Approved for public release; distribution is unlimited.

13. SUPPLEMENTARY NOTES

The contracting officer's representative (COR) is Peter Plostins, U.S. Army Research Laboratory, ATTN: AMSRD-ARL-WM-BC, Aberdeen Proving Ground, MD 21005-5069, telephone number (410) 306-0800.

14. ABSTRACT

The work reported here presents a nonlinear model predictive observer specialized to smart projectiles. The observer is based on a two-step process consisting of an initial state predictor followed by a state estimate corrector. We generate the predictor state by simply integrating the projectile's fixed plane equations of motion forward in time while the corrector step updates the state estimate by the minimization of the difference between measurements and model-predicted measurements over a finite duration of time in the past. Since the proposed method permits a general nonlinear representation of the projectile, the corrector step requires the solution of a nonlinear minimization problem which is subsequently solved with the use of a damped Newton procedure. The nonlinear model predictive observer is exercised on a smart projectile that employs a typical array of sensors including global positioning system, a three-axis gyroscope, three-axis accelerometers, and a three-axis magnetometer. Results with this smart weapon observer are promising since the observer is capable of estimating the full state of the projectile, including orientation and translational velocity, when realistic noise and bias errors are included in the sensor measurements. Relative to other existing observers, the proposed observer is computationally intensive because of the need to solve a nonlinear minimization problem at each computational cycle of the observer.

15. SUBJECT TERMS

nonlinear model; smart projectiles

16. SECURITY CLASSIFICATION OF:			17. LIMITATION OF ABSTRACT	18. NUMBER OF PAGES	19a. NAME OF RESPONSIBLE PERSON
a. REPORT	b. ABSTRACT	c. THIS PAGE			Peter Plostins
UNCLASSIFIED	UNCLASSIFIED	UNCLASSIFIED	SAR	30	19b. TELEPHONE NUMBER (*Include area code*) 410-306-0800

Standard Form 298 (Rev. 8/98)
Prescribed by ANSI Std. Z39.18

Contents

List of Figures iv

List of Tables iv

1. Introduction 1

2. Projectile Flight Dynamic Model 2

3. Sensor Model 5

4. Nonlinear Model Predictive Observer 6

5. Sample Results 9

6. Conclusions 11

7. References 21

Nomenclature 23

Distribution List 24

List of Figures

Figure 1. Position definitions. 2
Figure 2. Orientation definitions. 3
Figure 3. Measurement discretization. 7
Figure 4. Single time step iterations. 10
Figure 5. Trade study results. 11
Figure 6. Noise filtering. 12
Figure 7. Projectile range. 13
Figure 8. Projectile cross range. 13
Figure 9. Projectile altitude. 14
Figure 10. Projectile roll angle. 14
Figure 11. Projectile Euler angle θ. 15
Figure 12. Projectile Euler angle ψ. 15
Figure 13. Projectile velocity u. 16
Figure 14. Projectile velocity v. 16
Figure 15. Projectile velocity w. 17
Figure 16. Projectile rate p. 17
Figure 17. Projectile rate q. 18
Figure 18. Projectile rate r. 18
Figure 19. Estimate error in range. 19
Figure 20. Estimate error in ϕ. 19
Figure 21. Estimate error in u. 20
Figure 22. Estimate error in p. 20

List of Tables

Table 1. Sensor noise standard deviation. 10

1. Introduction

Smart projectiles promise to provide drastic improvements in impact point performance of artillery shells, mortars, grenades, and direct fire tank rounds. Although the potential benefit of these new weapons is quite substantial, the technological challenges are also difficult. In contrast to un-guided projectiles, smart projectiles must include hardware in the form of a sensor suite, a microprocessor, and a physical control mechanism along with associated software. These added components must be small to fit within geometric constraints and rugged to withstand the very harsh launch environment. To constrain cost, the number of on-board sensors must also be minimized. A key aspect of the flight control system software is the logic that blends available sensor data together to form a usable feedback signal for active control. This is the classic state estimator or observer problem. The state estimator is often a critical element within a smart weapon flight control system and generally affects impact performance of the weapon in a major way. The use of on-board sensors for projectile state observation is plagued by the noise inherent in physical sensors, while the use of on-board state propagators is plagued by inaccuracies inherent in simple dynamic models (*1*).

For almost 50 years, the work horse of state estimation has been the celebrated Kalman filter (*2 through 9*), which allows for a combination of imperfect sensor information and a linear model of the overall system to be blended in a manner that provides an optimal state estimate for linear systems. The extended Kalman filter (*10, 11*) is the typical way that estimators are designed for nonlinear physical systems. In the extended Kalman filter, the nonlinear system is effectively approximated by a linear system, and the standard Kalman filter is used on the linear system. Although Kalman filters and extended Kalman filters are used extensively in practice, they are not without problems. System errors and measurement errors in a Kalman filter are usually assumed to be zero-mean Gaussian process with a known covariance. Modeling errors seldom assume this form, and measurement error statistics are often not well known, leaving users to select error covariance in a trial-and-error fashion. This filter-tuning process can be time consuming. In some applications, it can be difficult to get the estimates to converge.

An alternative to a Kalman filter is a nonlinear observer that works directly with the nonlinear dynamic system and not a locally linearized approximation of the system. Because of a large number of applications, a significant literature base has amassed for nonlinear observers (*12, 13, 14*). Algebraic methods have been employed to transform certain classes of nonlinear systems into observer normal form, where observers can be constructed with guaranteed convergence properties. Another approach to construct nonlinear observers lies in variable structure systems theory. With the Lyapunov theory, extensions of standard linear observer theory can be made to prove asymptotic stability of nonlinear observers. It is also possible to employ model predictive control techniques to form nonlinear model predictive observers. The focus of the current report is

the use of a nonlinear model predictive observer to estimate the state of a smart projectile. The observer is based on a two-step process consisting of an initial state predictor followed by a state estimate corrector. We generate the predictor state by simply integrating the projectile's fixed plane equations of motion forward in time while the corrector step updates the state estimate by the minimization of the difference between measurements and model predicted measurements over a finite duration of time in the past. Since the proposed method permits a general nonlinear representation of the projectile, the corrector step requires the solution of a nonlinear minimization problem, which is subsequently solved with a damped Newton procedure. The nonlinear model predictive observer is exercised on a smart projectile that employs a typical array of sensors including global positioning system (GPS), a three-axis gyroscope, three-axis accelerometers, and a three-axis magnetometer. Trade-off studies are shown that vary the estimation horizon.

2. Projectile Flight Dynamic Model

A six-degree-of-freedom (6-DOF) rigid projectile model has been proved to accurately simulate the dynamics of a projectile in atmospheric flight (*15*). The 6 DOF are comprised of the three translational components describing the position of the projectile's center of mass and the three Euler angles describing the orientation of the projectile with respect to a fixed inertial axis. Figures 1 and 2 provide a schematic of the degrees of freedom.

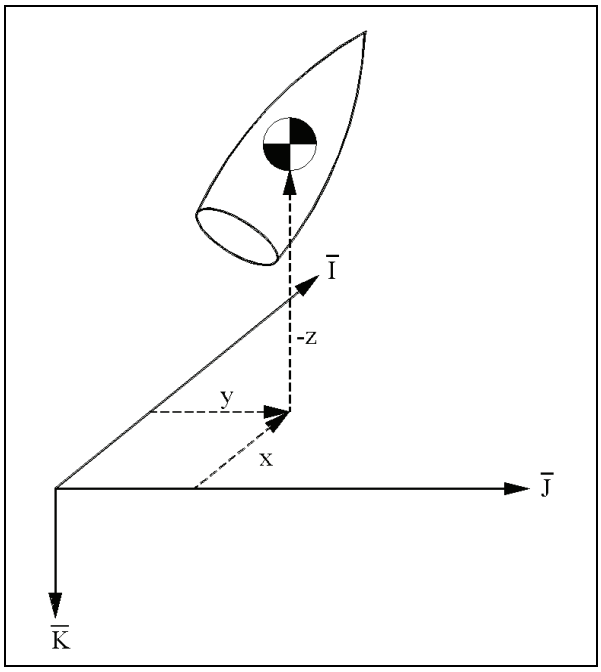

Figure 1. Position definitions.

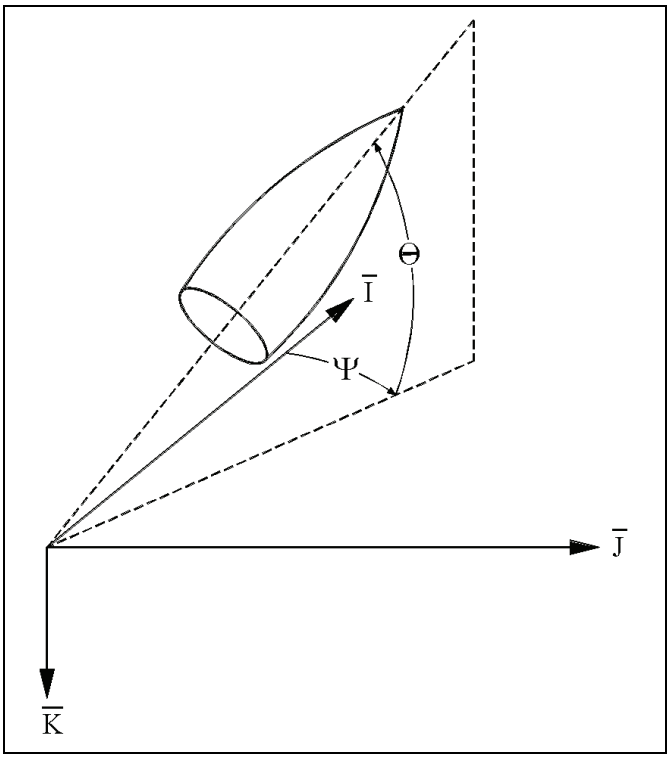

Figure 2. Orientation definitions.

Although commonly expressed and computed in the projectile body frame, the equations of motion for the 6-DOF model are expressed in the no-roll frame to reduce computational requirements within the observer.

$$\begin{Bmatrix} \dot{x} \\ \dot{y} \\ \dot{z} \end{Bmatrix} = \begin{bmatrix} c_\theta c_\psi & -s_\psi & s_\theta c_\psi \\ c_\theta s_\psi & c_\psi & s_\theta s_\psi \\ -s_\theta & 0 & c_\theta \end{bmatrix} \begin{Bmatrix} \tilde{u} \\ \tilde{v} \\ \tilde{w} \end{Bmatrix} \tag{1}$$

$$\begin{Bmatrix} \dot{\phi} \\ \dot{\theta} \\ \dot{\psi} \end{Bmatrix} = \begin{bmatrix} 1 & 0 & t_\theta \\ 0 & 1 & 0 \\ 0 & 0 & 1/c_\theta \end{bmatrix} \begin{Bmatrix} \tilde{p} \\ \tilde{q} \\ \tilde{r} \end{Bmatrix} \tag{2}$$

$$\begin{Bmatrix} \dot{\tilde{u}} \\ \dot{\tilde{v}} \\ \dot{\tilde{w}} \end{Bmatrix} = \begin{Bmatrix} \tilde{X}/m \\ \tilde{Y}/m \\ \tilde{Z}/m \end{Bmatrix} + \begin{Bmatrix} \tilde{r}\tilde{v} - \tilde{q}\tilde{w} \\ -t_\theta \tilde{r}\tilde{w} - \tilde{r}\tilde{u} \\ \tilde{q}\tilde{u} + t_\theta \tilde{r}\tilde{v} \end{Bmatrix} \tag{3}$$

$$\begin{Bmatrix} \dot{\tilde{p}} \\ \dot{\tilde{q}} \\ \dot{\tilde{r}} \end{Bmatrix} = [I]^{-1} \left(\begin{Bmatrix} \tilde{L} \\ \tilde{M} \\ \tilde{N} \end{Bmatrix} + \begin{bmatrix} 0 & -\tilde{r} & \tilde{q} \\ \tilde{r} & 0 & \tilde{r}t_\theta \\ -\tilde{q} & -\tilde{r}t_\theta & 0 \end{bmatrix} [I] \begin{Bmatrix} \tilde{p} \\ \tilde{q} \\ \tilde{r} \end{Bmatrix} \right) \tag{4}$$

The force acting on the projectile in equation 3 is comprised of the weight force (W) and the aerodynamic force. The aerodynamic force is split into a standard (A) and Magnus (M) aerodynamic force. The combination of forces is expressed in equation 5.

$$\begin{Bmatrix} \tilde{X} \\ \tilde{Y} \\ \tilde{Z} \end{Bmatrix} = \begin{Bmatrix} \tilde{X}_w \\ \tilde{Y}_w \\ \tilde{Z}_w \end{Bmatrix} + \begin{Bmatrix} \tilde{X}_A \\ \tilde{Y}_A \\ \tilde{Z}_A \end{Bmatrix} + \begin{Bmatrix} \tilde{X}_M \\ \tilde{Y}_M \\ \tilde{Z}_M \end{Bmatrix} \tag{5}$$

Equation 6 provides the expression for the weight force in the no-roll coordinate system.

$$\begin{Bmatrix} \tilde{X}_w \\ \tilde{Y}_w \\ \tilde{Z}_w \end{Bmatrix} = mg \begin{Bmatrix} -s_\theta \\ 0 \\ c_\theta \end{Bmatrix} \tag{6}$$

Equation 7 provides the expression for the aerodynamic force in the no-roll coordinate system. This force acts upon the projectile at the aerodynamic center of pressure.

$$\begin{Bmatrix} \tilde{X}_A \\ \tilde{Y}_A \\ \tilde{Z}_A \end{Bmatrix} = -\frac{\pi}{8} \rho {V_A}^2 D^2 \begin{Bmatrix} C_{X0} + C_{X2}\alpha^2 + C_{X2}\beta^2 \\ C_{Y0} + C_{YB1}\beta \\ C_{Z0} + C_{ZA1}\alpha \end{Bmatrix} \tag{7}$$

Equation 8 provides the expression for the Magnus force in the no-roll coordinate system. The Magnus force acts upon the projectile at the Magnus force center of pressure.

$$\begin{Bmatrix} \tilde{X}_M \\ \tilde{Y}_M \\ \tilde{Z}_M \end{Bmatrix} = \frac{\pi}{8} \rho {V_A}^2 D^2 \begin{Bmatrix} 0 \\ \dfrac{\tilde{p} D C_{NPA} \alpha}{2V_A} \\ \dfrac{-\tilde{p} D C_{NPA} \beta}{2V_A} \end{Bmatrix} \tag{8}$$

Equations 7 and 8 are based on Mach number-dependent coefficients, the aerodynamic angles of attack, and the total aerodynamic velocity.

The moment acting on the projectile in equation 4 is comprised of the moment attributable to the standard aerodynamic force (A), the moment attributable to the Magnus aerodynamic force (M) and the unsteady aerodynamic moments (UA) as shown in equation 9.

$$\begin{Bmatrix} \tilde{L} \\ \tilde{M} \\ \tilde{N} \end{Bmatrix} = \begin{Bmatrix} \tilde{L}_A \\ \tilde{M}_A \\ \tilde{N}_A \end{Bmatrix} + \begin{Bmatrix} \tilde{L}_M \\ \tilde{M}_M \\ \tilde{N}_M \end{Bmatrix} + \begin{Bmatrix} \tilde{L}_{UA} \\ \tilde{M}_{UA} \\ \tilde{N}_{UA} \end{Bmatrix} \tag{9}$$

The moment attributable to the aerodynamic force is expressed in equation 10.

$$\begin{Bmatrix} \tilde{L}_A \\ \tilde{M}_A \\ \tilde{N}_A \end{Bmatrix} = \begin{bmatrix} 0 & -R_{\oplus CAZ} & R_{\oplus CAY} \\ R_{\oplus CAZ} & 0 & -R_{\oplus CAX} \\ -R_{\oplus CAY} & R_{\oplus CAX} & 0 \end{bmatrix} \begin{Bmatrix} \tilde{X}_A \\ \tilde{Y}_A \\ \tilde{Z}_A \end{Bmatrix} \tag{10}$$

The moment attributable to the Magnus force is expressed in equation 11.

$$\begin{Bmatrix} \tilde{L}_M \\ \tilde{M}_M \\ \tilde{N}_M \end{Bmatrix} = \begin{bmatrix} 0 & -R_{\oplus CMZ} & R_{\oplus CMY} \\ R_{\oplus CMZ} & 0 & -R_{\oplus CMX} \\ -R_{\oplus CMY} & R_{\oplus CMX} & 0 \end{bmatrix} \begin{Bmatrix} \tilde{X}_M \\ \tilde{Y}_M \\ \tilde{Z}_M \end{Bmatrix} \tag{11}$$

The unsteady aerodynamic moments acting on the projectile are expressed in equation 12.

$$\begin{Bmatrix} \tilde{L}_{UA} \\ \tilde{M}_{UA} \\ \tilde{N}_{UA} \end{Bmatrix} = \frac{\pi}{8} \rho {V_A}^2 D^3 \begin{Bmatrix} C_{DD} + \dfrac{\tilde{p} DC_{LP}}{2V_A} \\ \dfrac{\tilde{q} DC_{MQ}}{2V_A} \\ \dfrac{\tilde{r} DC_{NR}}{2V_A} \end{Bmatrix} \tag{12}$$

These coefficients are projectile specific functions of the Mach number of the projectile.

3. Sensor Model

Within the corrector part of the observer, estimated motion of the projectile is contrasted with a given sensor suite to iteratively determine state estimates. Sensor suites on a smart weapon typically include gyroscope, accelerometer, magnetometer, and GPS measurements. To properly blend these data together in the observer, an analytical sensor model is required for each sensor type, which relates sensor readings to projectile motion via rigid body kinematics. Major error sources such as noise error, bias error, scale factor error, cross-axis sensitivity/misalignment, and sensor misposition can significantly affect sensor readings and must therefore be included in the sensor model. The acceleration experienced by the location of an accelerometer is

$$a_i = a_{Ni} + a_{Bi} + \vec{s}_{Ai}{}^T \left[R_S \right] \left(\left[S \right] \left(C_B \left(\vec{r}_{P \to Si} \right) + \begin{Bmatrix} \delta_{Si}^x \\ \delta_{Si}^y \\ \delta_{Si}^z \end{Bmatrix} \right) - g \begin{Bmatrix} -s_\theta \\ s_\phi c_\theta \\ c_\phi c_\theta \end{Bmatrix} \right) \tag{13}$$

where $\begin{Bmatrix} \vec{s}_{Ax}{}^T \\ \vec{s}_{Ay}{}^T \\ \vec{s}_{Ax}{}^T \end{Bmatrix} = \begin{bmatrix} s_{Ax} & c_{Ax}^{y} & c_{Ax}^{z} \\ c_{Ay}^{x} & s_{Ay} & c_{Ay}^{z} \\ c_{Az}^{x} & c_{Az}^{y} & s_{Az} \end{bmatrix}$ and $[S] = S_B(\vec{\alpha}_{B/I}) + S_B(\vec{\omega}_{B/I}) S_B(\vec{\omega}_{B/I})$

Also, the angular velocity of the gyroscopes is

$$\begin{Bmatrix} \omega_x \\ \omega_y \\ \omega_z \end{Bmatrix} = \begin{Bmatrix} \omega_{Nx} \\ \omega_{Ny} \\ \omega_{Nz} \end{Bmatrix} + \begin{Bmatrix} \omega_{Bx} \\ \omega_{By} \\ \omega_{Bz} \end{Bmatrix} + \begin{bmatrix} s_{Gx} & c_{Gx}^{y} & c_{Gx}^{z} \\ c_{Gy}^{x} & s_{Gy} & c_{Gy}^{z} \\ c_{Gz}^{x} & c_{Gz}^{y} & s_{Gz} \end{bmatrix} [R_S] \begin{Bmatrix} p \\ q \\ r \end{Bmatrix} \tag{14}$$

Magnetometers measure the dot product between the earth's magnetic field vector and the sensitive axis of the magnetometer. Although they do not directly measure any rigid projectile model states, three magnetometers can be arranged orthogonally so that they project the earth's magnetic field vector onto the projectile body frame and aid in estimating projectile orientation.

$$\begin{Bmatrix} M_X \\ M_Y \\ M_Z \end{Bmatrix} = \begin{Bmatrix} M_{NX} \\ M_{NY} \\ M_{NZ} \end{Bmatrix} + [R_S] \begin{bmatrix} c_\theta c_\psi & s_\phi s_\theta c_\psi - c_\phi s_\psi & c_\phi s_\theta c_\psi - s_\phi s_\psi \\ c_\theta s_\psi & s_\phi s_\theta s_\psi - c_\phi c_\psi & c_\phi s_\theta s_\psi - s_\phi c_\psi \\ -s_\theta & s_\phi c_\theta & c_\phi c_\theta \end{bmatrix}^T \begin{Bmatrix} E_X \\ E_Y \\ E_Z \end{Bmatrix} \tag{15}$$

GPS measures the position and velocity of the receiver relative to the earth, which is given by the following:

$$\begin{Bmatrix} G_x \\ G_y \\ G_z \end{Bmatrix} = \begin{Bmatrix} G_{Nx} \\ G_{Ny} \\ G_{Nz} \end{Bmatrix} + \begin{Bmatrix} G_{Bx} \\ G_{By} \\ G_{Bz} \end{Bmatrix} + \begin{Bmatrix} x \\ y \\ z \end{Bmatrix}$$
$$\begin{Bmatrix} G_{\dot{x}} \\ G_{\dot{y}} \\ G_{\dot{z}} \end{Bmatrix} = \begin{Bmatrix} G_{N\dot{x}} \\ G_{N\dot{y}} \\ G_{N\dot{z}} \end{Bmatrix} + \begin{Bmatrix} G_{B\dot{x}} \\ G_{B\dot{y}} \\ G_{B\dot{z}} \end{Bmatrix} + \begin{Bmatrix} \dot{x} \\ \dot{y} \\ \dot{z} \end{Bmatrix} \tag{16}$$

4. Nonlinear Model Predictive Observer

Consider the projectile dynamic system just described. Using the state vector defined by $x = \{x, y, z\phi, \theta, \psi, \tilde{u}, \tilde{v}, \tilde{w}, \tilde{p}, \tilde{q}, \tilde{r}\}^T$, we can describe the dynamic system by the following:

$$\dot{x} = f(x) \tag{17}$$

Assuming that several quantities are measured that are related to the state so that the output is described by the following:

$$y = h(x) \tag{18}$$

It is desired to estimate the state x at any time with the use of the math model and measurements. The state estimate will be called $\tilde{x}$ and the measurement reconstruction uses the estimates $\tilde{y} = h(\tilde{x})$. In order to make a state estimate, a quadratic cost function is minimized over a discrete horizon (see figure 3).

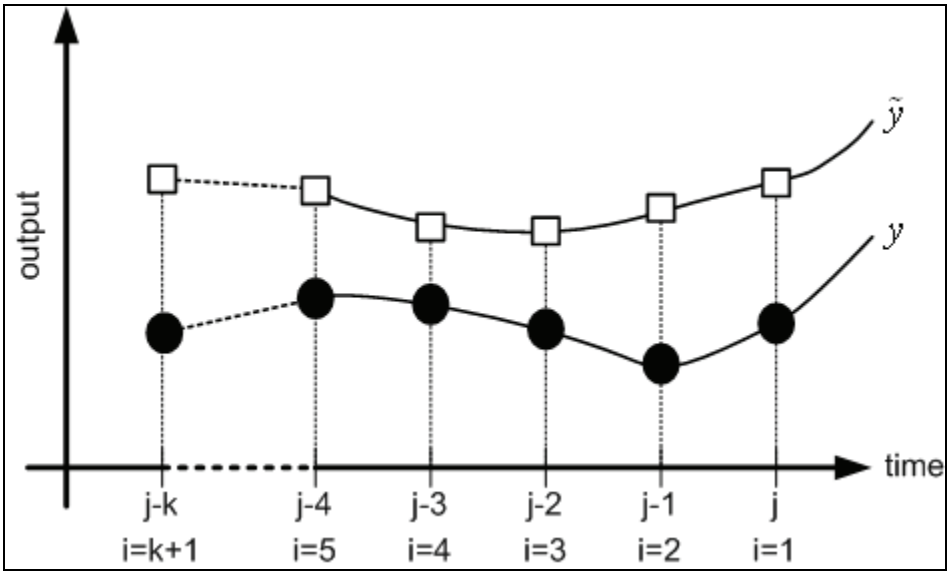

Figure 3. Measurement discretization.

$$J = \frac{1}{2}\sum_{i=1}^{k+1}\left[\tilde{y}(\tilde{x}_i) - y(x_i)\right]^T W\left[\tilde{y}(\tilde{x}_i) - y(x_i)\right] \tag{19}$$

where W is positive definite and k is the selected measurement horizon.

In solving the minimization problem, it is desirable to express the cost function as a function of the state estimate at *j*. Equation 20 shows the cost function as it relates to the current state estimate.

$$J = \frac{1}{2}\sum_{i=1}^{k+1}\left[g_i(\tilde{x}_j) - y(x_i)\right]^T W\left[g_i(\tilde{x}_j) - y(x_i)\right] \tag{20}$$

$g_i(\tilde{x}_j)$ is a function that relates the state estimate at the current time to past sensor measurements. Its structure is discussed later in this report.

For the state estimate to be an optimal solution, the cost function must satisfy the gradient condition.

$$\frac{\partial J}{\partial \tilde{x}} = 0 \tag{21}$$

In order to satisfy equation 21, a numerical technique is used because J is highly nonlinear. A Newton type method is used to solve for $\tilde{x}$ that will drive $\partial J/\partial \tilde{x} = 0$. To achieve this condition

numerically, J is approximated as a local quadratic function (equation 22), and a perturbation on the state is solved for so that the gradient of the local model is zero (equation 23).

$$J \approx J_0 + \left.\frac{\partial J}{\partial \tilde{x}}\right|_{\tilde{x}_0} \left(\tilde{x}_N - \tilde{x}_0\right) + \frac{1}{2}\left(\tilde{x}_N - \tilde{x}_0\right)^T \left.\frac{\partial^2 J}{\partial \tilde{x}^2}\right|_{\tilde{x}_0} \left(\tilde{x}_N - \tilde{x}_0\right) \tag{22}$$

$$\frac{\partial J}{\partial \tilde{x}_N} = \left.\frac{\partial J}{\partial \tilde{x}}\right|_{\tilde{x}_0} + \left.\frac{\partial^2 J}{\partial \tilde{x}^2}\right|_{\tilde{x}_0} \left(\tilde{x}_N - \tilde{x}_0\right) = 0 \tag{23}$$

The line search parameter α is implemented in order to accelerate convergence (equation 24):

$$\tilde{x}_N = \tilde{x}_0 - \alpha \left[\left.\frac{\partial^2 J}{\partial \tilde{x}^2}\right|_{\tilde{x}_0}\right]^{-1} \left.\frac{\partial J}{\partial \tilde{x}}\right|_{\tilde{x}_0} \tag{24}$$

When a set of nonlinear equations is solved iteratively, a starting guess is required. This initial guess is generated by integrating the equations of motion (1 through 4) forward one time step. This can be viewed as the predictor step, and solving the nonlinear equations can be viewed as the corrector step.

A key aspect of this technique is linking the output at one point in time to the state at the time of interest. To create this link, the dynamic equations of motion can be used and applied with a suitable discretization. For this problem, Euler's formula was used for its simplicity and ease of computation.

$$\tilde{x}_{j-1} = \tilde{x}_j - \Delta t f\left(\tilde{x}_j\right) \tag{25}$$

This link can be used recursively to link the state at any two times.

$$\begin{aligned} \tilde{x}_{j-2} &= \tilde{x}_{j-1} - \Delta t f\left(\tilde{x}_{j-1}\right) = \tilde{x}_j - \Delta t f\left(\tilde{x}_j\right) - \Delta t f\left(\tilde{x}_j - \Delta t f\left(\tilde{x}_j\right)\right) \\ \tilde{x}_{j-3} &= \tilde{x}_j - \Delta t f\left(\tilde{x}_j\right) - \Delta t f\left(\tilde{x}_j - \Delta t f\left(\tilde{x}_j\right)\right) - \Delta t f\left(\tilde{x}_j - \Delta t f\left(\tilde{x}_j\right) - \Delta t f\left(\tilde{x}_j - \Delta t f\left(\tilde{x}_j\right)\right)\right) \end{aligned} \tag{26}$$

Equation 24 requires the partial derivatives of the measurements. These derivatives can be computed numerically, partially numerically, and partially analytically, or completely analytically. Using the analytical approach, we get the following equations:

$$\begin{aligned} \frac{\partial J}{\partial \tilde{x}_j} &= \sum_{i=1}^{k+1} \left[\frac{\partial \tilde{y}\left(\tilde{x}_i\right)}{\partial \tilde{x}_j}\right]^T W\left(\tilde{y}\left(\tilde{x}_i\right) - y\left(x_i\right)\right) + \left(\tilde{y}\left(\tilde{x}_i\right) - y\left(x_i\right)\right)^T W \frac{\partial \tilde{y}\left(\tilde{x}_i\right)}{\partial \tilde{x}_j} \\ \frac{\partial^2 J}{\partial \tilde{x}_j^2} &= \sum_{i=1}^{k+1} \left[\frac{\partial^2 \tilde{y}\left(\tilde{x}_i\right)}{\partial \tilde{x}_j^2}\right]^T W\left(\tilde{y}\left(\tilde{x}_i\right) - y\left(x_i\right)\right) + 2\left[\frac{\partial \tilde{y}\left(\tilde{x}_i\right)}{\partial \tilde{x}_j}\right]^T W \frac{\partial \tilde{y}\left(\tilde{x}_i\right)}{\partial \tilde{x}_j} + \left(\tilde{y}\left(\tilde{x}_i\right) - y\left(x_i\right)\right)^T W \frac{\partial^2 \tilde{y}\left(\tilde{x}_i\right)}{\partial \tilde{x}_j^2} \end{aligned} \tag{27}$$

The second partial derivatives used in equation 27 can typically be neglected because they are very small when compared with the first partial derivative term (*16*).

Equation 27 requires more derivatives to be determined.

$$\begin{aligned}\frac{\partial \tilde{y}\left(\tilde{x}_{j-1}\right)}{\partial \tilde{x}_j} &= \frac{\partial \tilde{y}\left(\tilde{x}_{j-1}\right)}{\partial \tilde{x}_{j-1}} \frac{\partial \tilde{x}_{j-1}}{\partial \tilde{x}_j} \\ &= \left.\frac{\partial h}{\partial \tilde{x}}\right|_{\tilde{x}_{j-1}} \frac{\partial}{\partial \tilde{x}_j}\left(\tilde{x}_j - \Delta t f\left(\tilde{x}_j\right)\right) \\ &= \left.\frac{\partial h}{\partial \tilde{x}}\right|_{\tilde{x}_{j-1}} \left(I - \Delta t \left.\frac{\partial f}{\partial \tilde{x}}\right|_{\tilde{x}_j}\right)\end{aligned} \tag{28}$$

These derivatives can also be recursive.

$$\frac{\partial \tilde{y}\left(\tilde{x}_{j-2}\right)}{\partial \tilde{x}_j} = \frac{\partial \tilde{y}\left(\tilde{x}_{j-2}\right)}{\partial \tilde{x}_{j-2}} \frac{\partial \tilde{x}_{j-2}}{\partial \tilde{x}_{j-1}} \frac{\partial \tilde{x}_{j-1}}{\partial \tilde{x}_j} \tag{29}$$

$$\frac{\partial y\left(\tilde{x}_{j-N}\right)}{\partial \tilde{x}_j} = \left.\frac{\partial h}{\partial x}\right|_{\tilde{x}_{j-N}} \prod_{p=1}^{N}\left(I - \Delta t \left.\frac{\partial f}{\partial \tilde{x}}\right|_{\tilde{x}_{j-N+p}}\right) \tag{30}$$

5. Sample Results

In order to exercise the methodology developed here, simulation results are generated for a sample system. The projectile considered is a typical 155-mm spin-stabilized projectile. The projectile is assumed to have a sensor suite on board which includes GPS, a three-axis accelerometer, a three-axis magnetometer, and a three-axis gyroscope.

Convergence of the corrector portion of the observer is shown in figure 4 for a single instant in time for a single magnetometer axis. In figure 4, a total of 15 points is used in the estimation horizon, and the numerical solution exhibits rapid convergence. The cost J with a guess at initial conditions was 7.1735e+004 and was reduced to 1.9027977e-001 and 1.9027976e-001 after estimates 4 and 5, respectively. The cost had not only converged, but the estimated output was very acceptable for the entire horizon. These results are typical for all measurements.

A trade study was conducted to determine an appropriate number of points in the measurement horizon *k*. A number of various horizons were selected, ranging from three data points to 42 data points. The measurement data were populated with noise with standard deviations shown in table 1 and remained the same for each case in the study. Also, the initial conditions at $j = 1$ were the same for each case of the study. The results of this trade study are shown in the figure 5. As the number of points in the prediction increases, the sensor noise becomes increasingly filtered. From this trade

study, it was determined that a horizon of 21 data points gave satisfactory estimates without requiring intense computations.

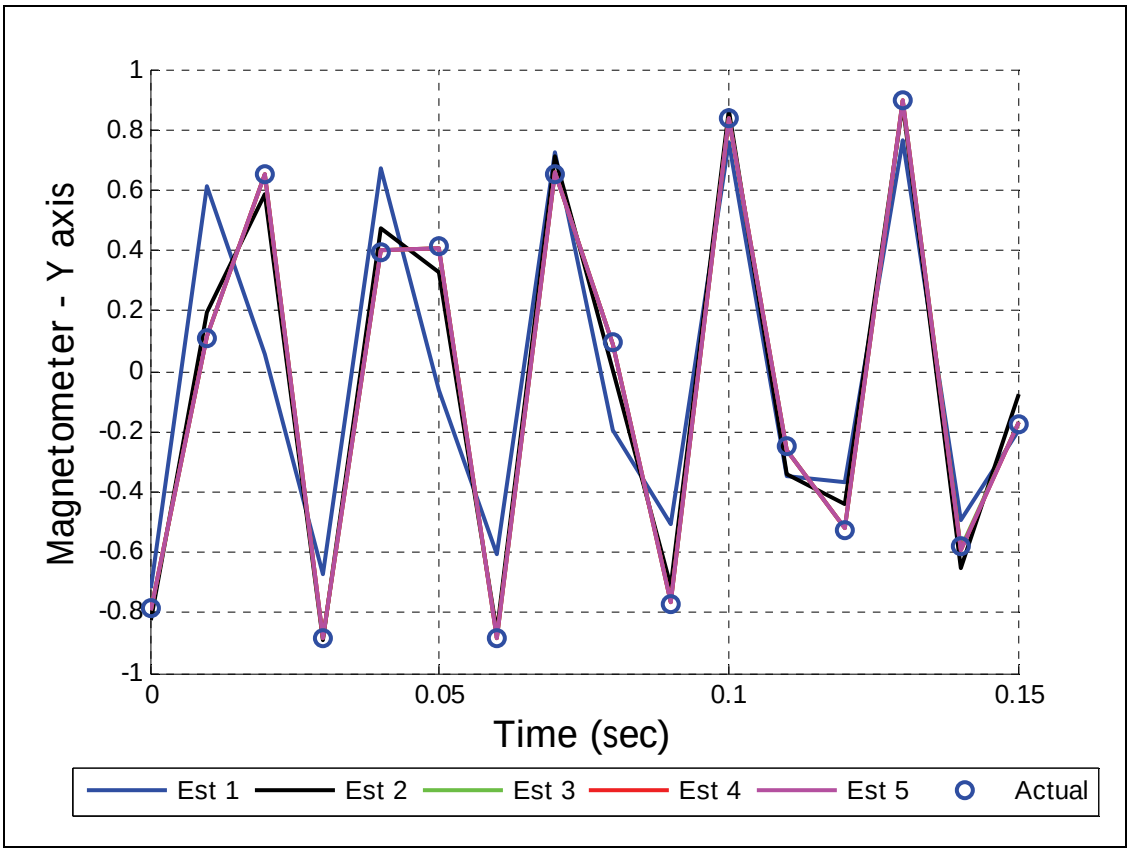

Figure 4. Single time step iterations.

Table 1. Sensor noise standard deviation.

Sensor	**Noise Standard Deviation**	**Sensor**	**Noise Standard Deviation**
GPS		Accelerometer	
x	4.8 ft	x -axis	0.03 ft/sec^2
y	4.8 ft	y -axis	0.03 ft/sec^2
z	10.8 ft	z -axis	0.03 ft/sec^2
$\dot{x}$	0.6 ft/sec	Magnetometer	
$\dot{y}$	0.6 ft/sec	x -axis	0.001
$\dot{z}$	0.6 ft/sec	y -axis	0.001
Gyroscope		z -axis	0.001
p	0.1 rad/sec		
q	0.1 rad/sec		
r	0.1 rad/sec		

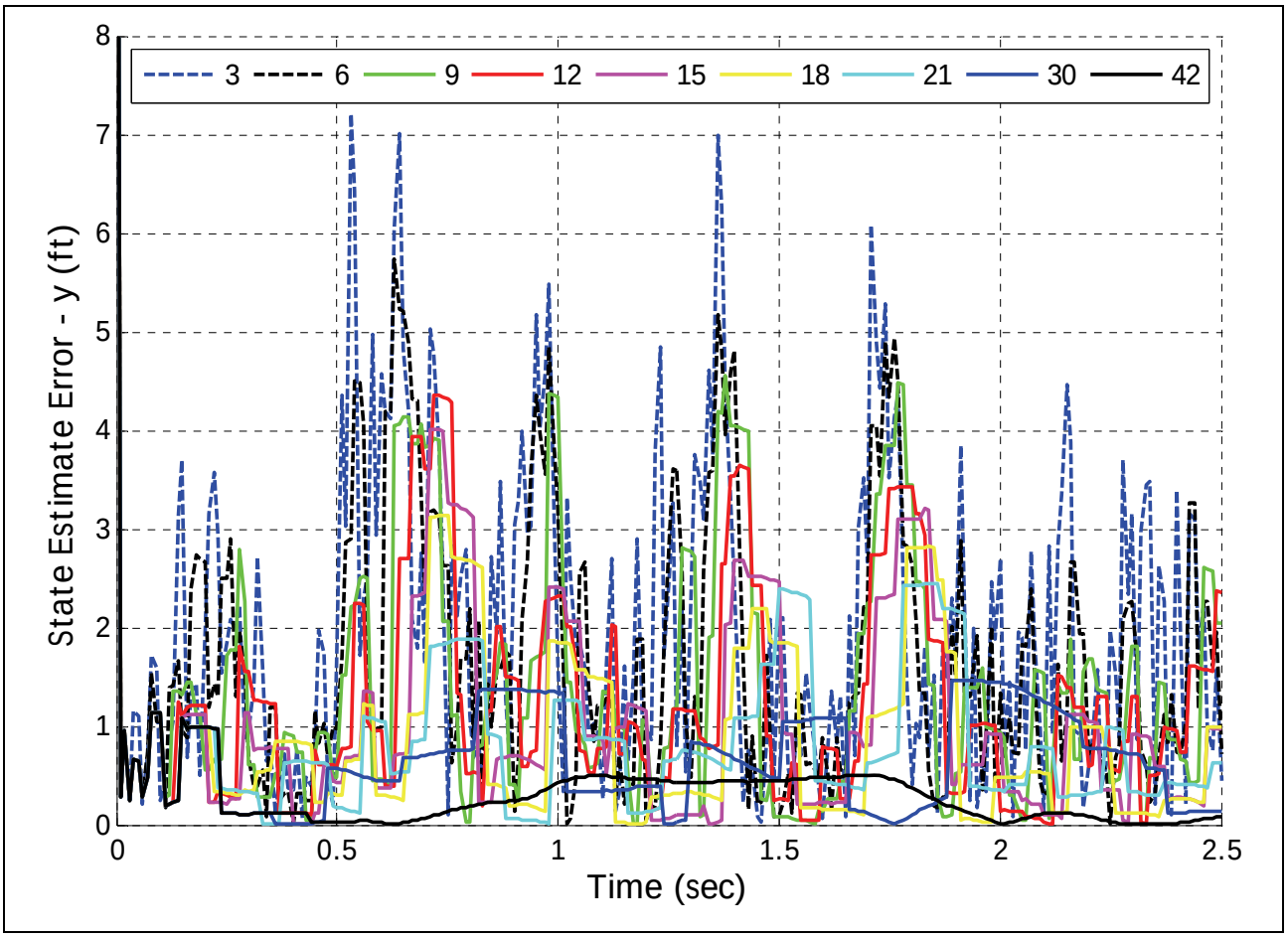

Figure 5. Trade study results.

To further illustrate how greatly this estimator can reduce to amplitude and frequency of noise, figure 6 compares the sensor output, estimated state, and actual state for a single GPS signal.

With a measurement horizon of 21 points, state estimates were found over a full projectile trajectory. The comparisons of each of the states with the state estimates are plotted in figures 7 through 22. Also plotted are the some of the errors between the actual state and the state estimate along the trajectory.

6. Conclusions

A nonlinear model predictive observer specialized to smart projectiles reported here can successfully predict the full state vector of a projectile trajectory. The observer is based on a two-step process consisting of an initial state predictor followed by a state estimate corrector. We generate the predictor state by simply integrating the projectile's fixed plane equations of motion forward in time while the corrector step updates the state estimate by the minimization of the difference

between measurements and model predicted measurements over a finite duration of time in the past. Since the method permits a general nonlinear representation of the projectile, the corrector step requires the solution of a nonlinear minimization problem which is subsequently solved with a damped Newton procedure. The nonlinear model predictive observer is exercised on a smart projectile that employs a typical array of sensors including GPS, a three-axis gyroscope, three-axis accelerometers, and a three-axis magnetometer. Results with this smart weapon observer are promising since the observer is capable of estimating the full state of the projectile, including orientation and translational velocity, when realistic noise and bias errors are included in the sensor measurements. Relative to other existing observers, however, the proposed observer is computationally intensive because of the need to solve a nonlinear minimization problem at each computation cycle of the observer.

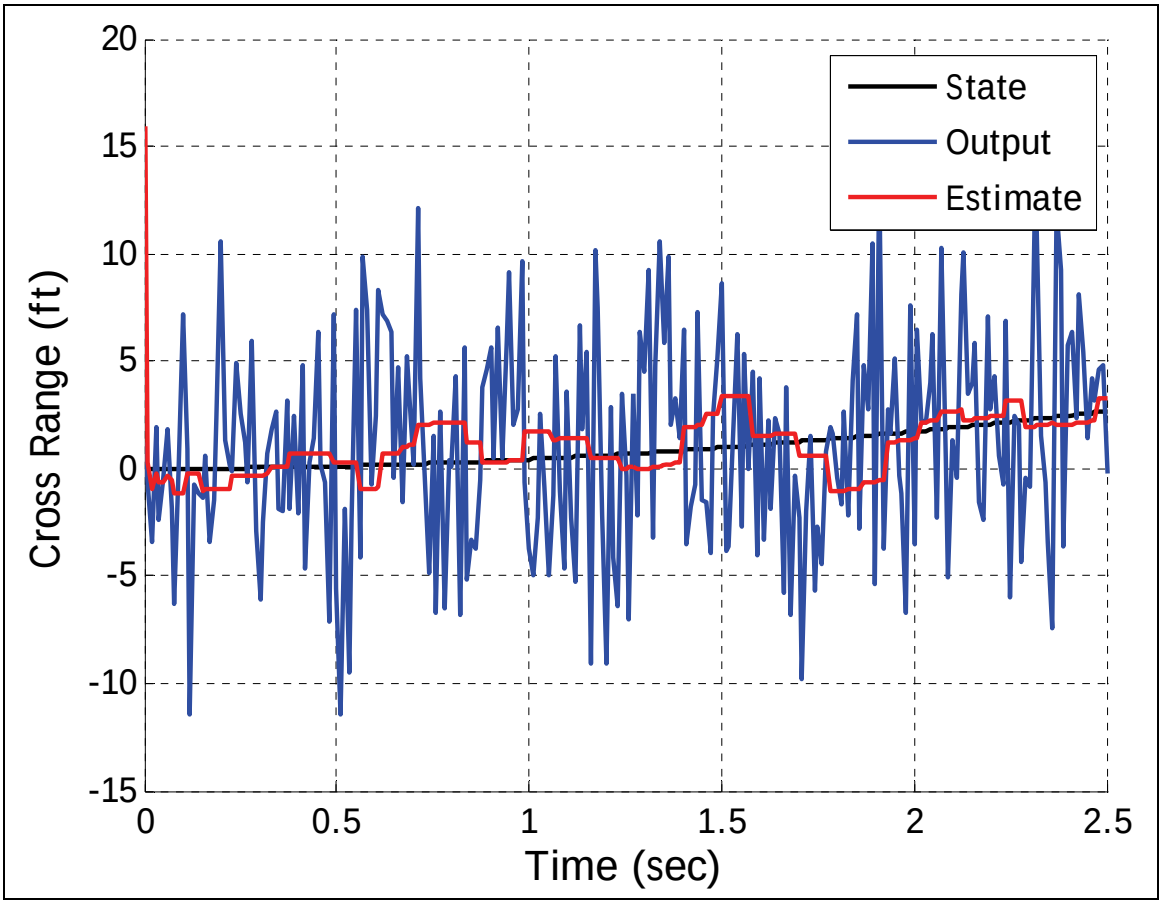

Figure 6. Noise filtering.

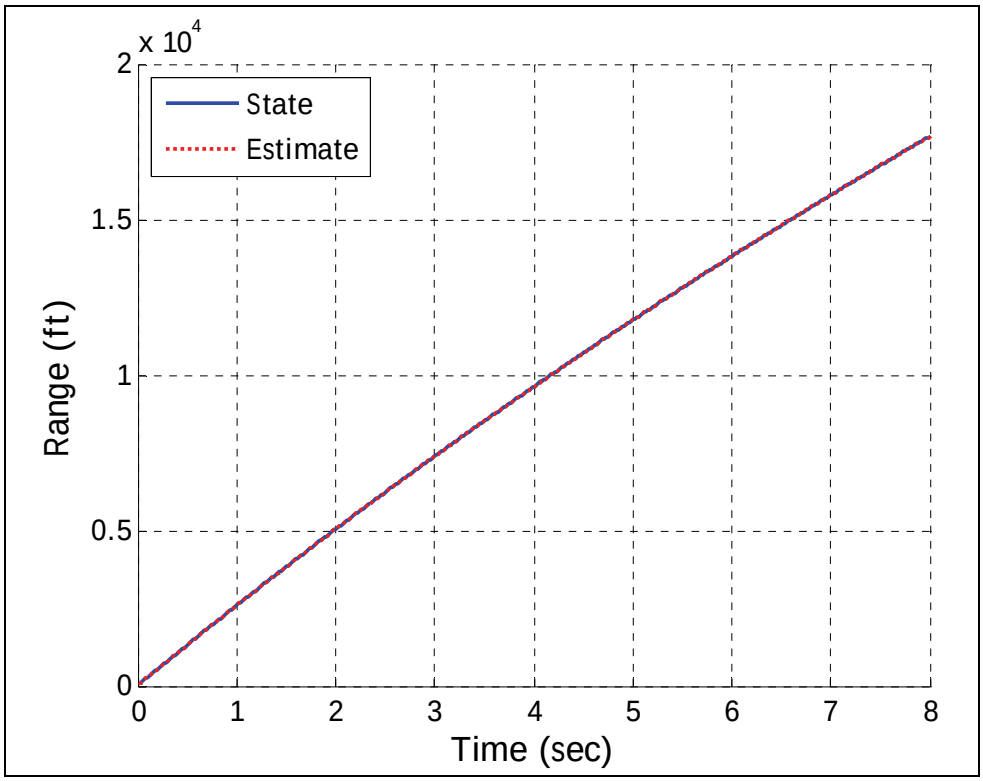

Figure 7. Projectile range.

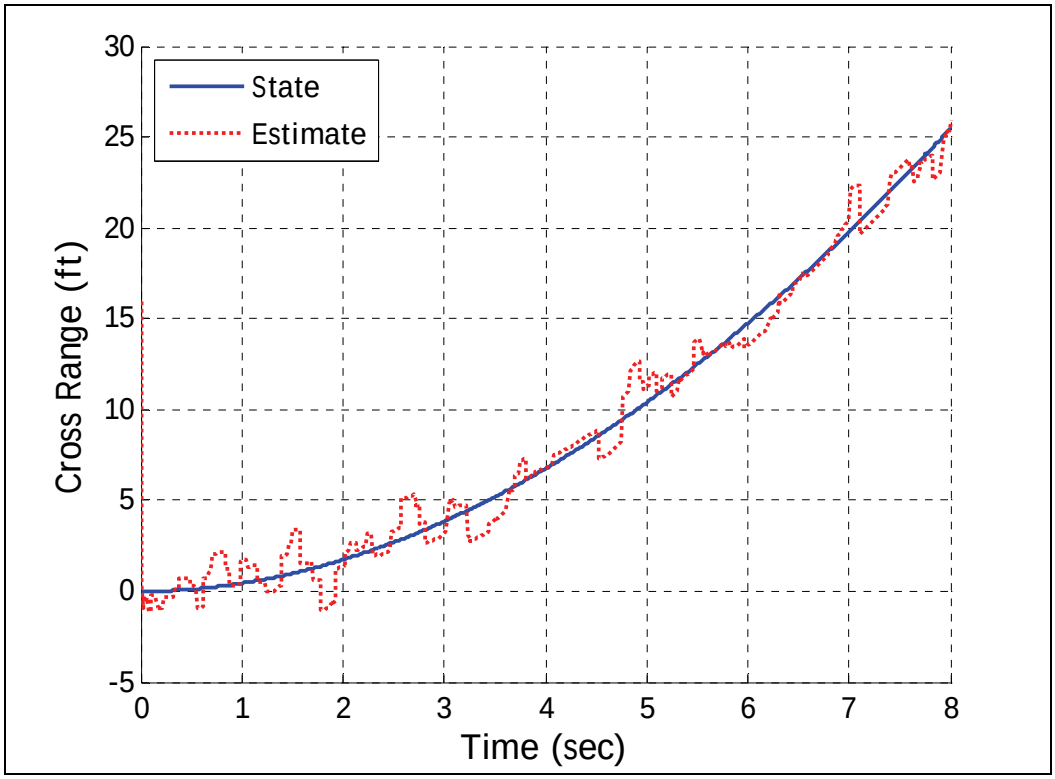

Figure 8. Projectile cross range.

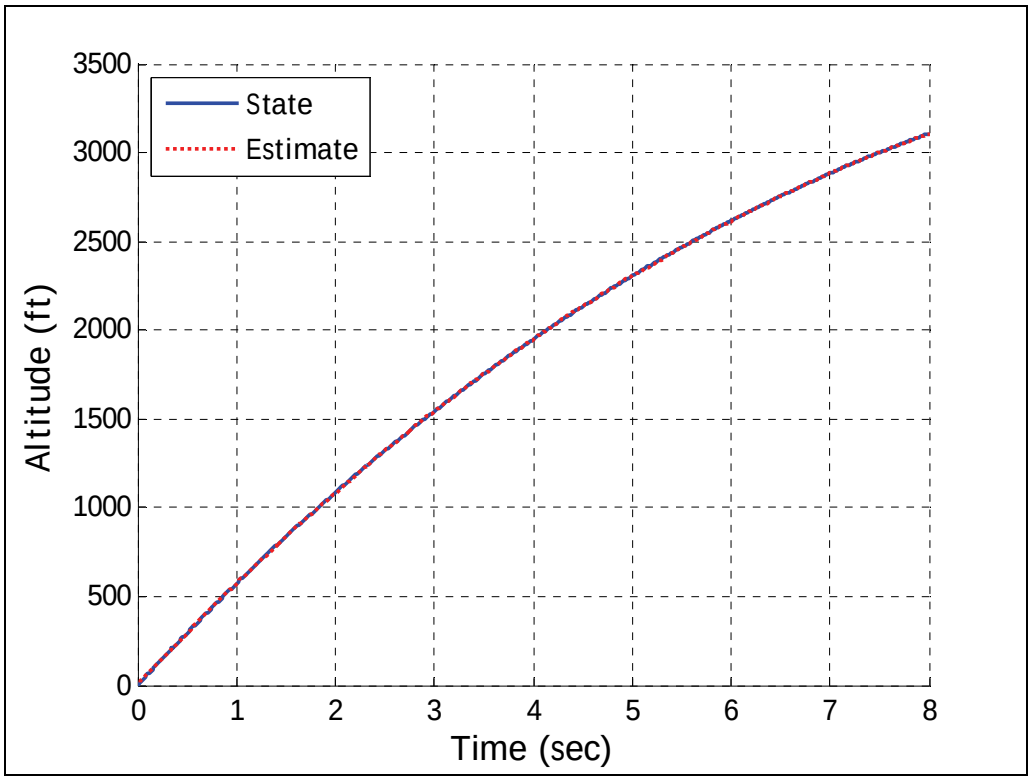

Figure 9. Projectile altitude.

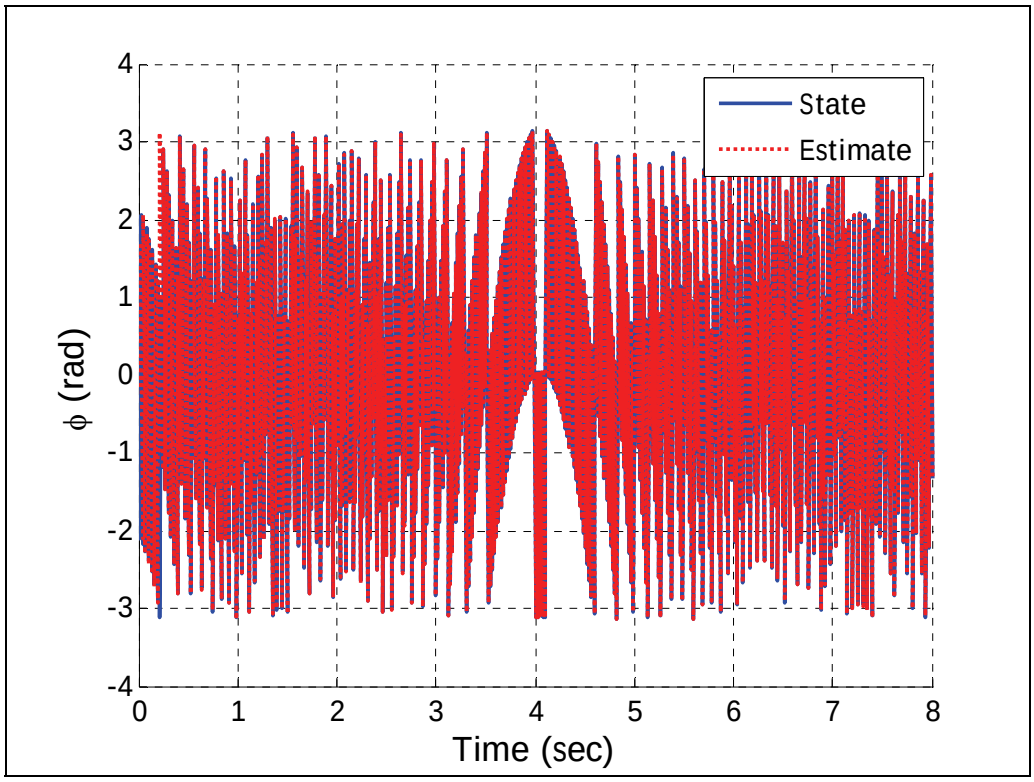

Figure 10. Projectile roll angle.

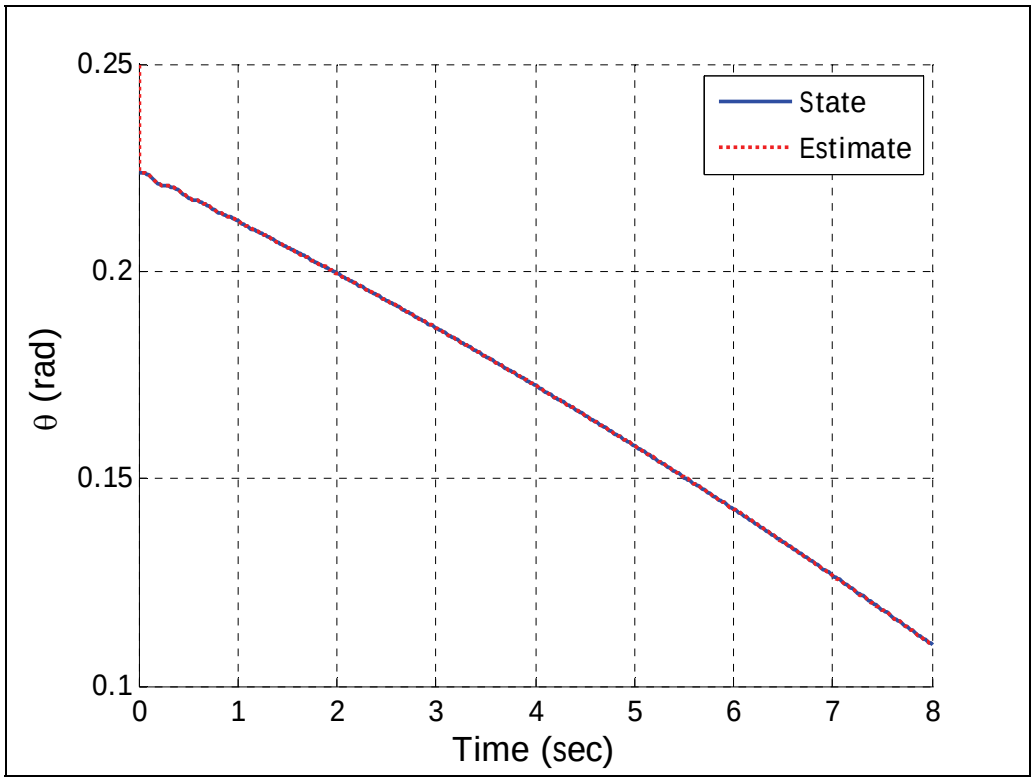

Figure 11. Projectile Euler angle θ.

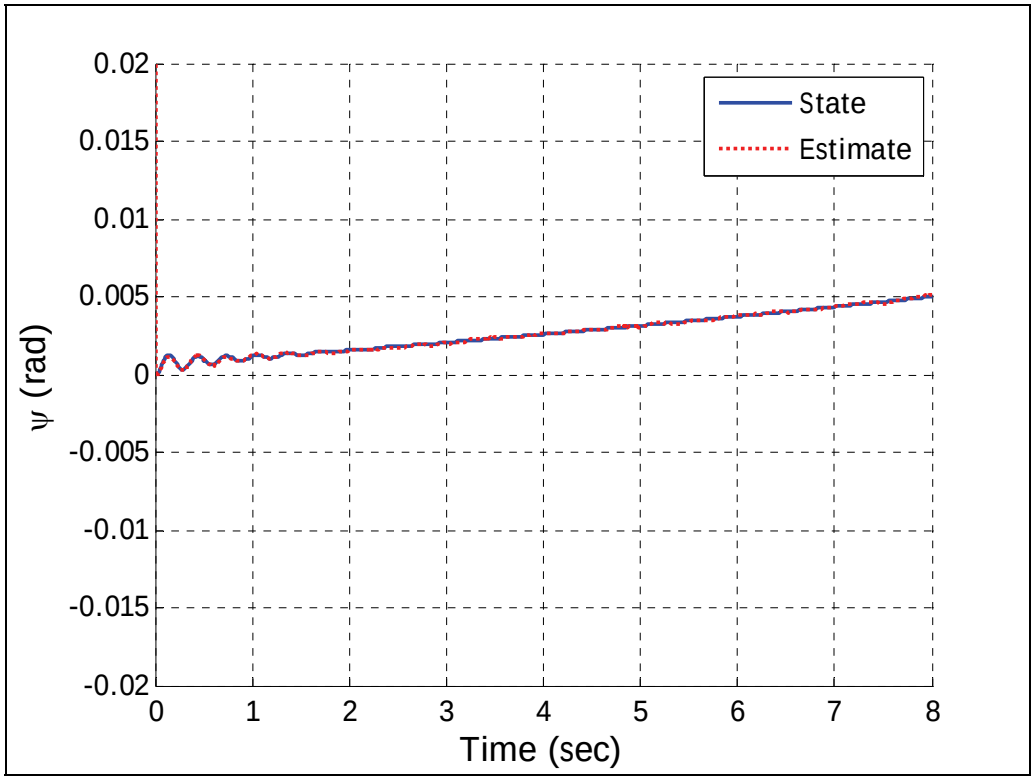

Figure 12. Projectile Euler angle ψ.

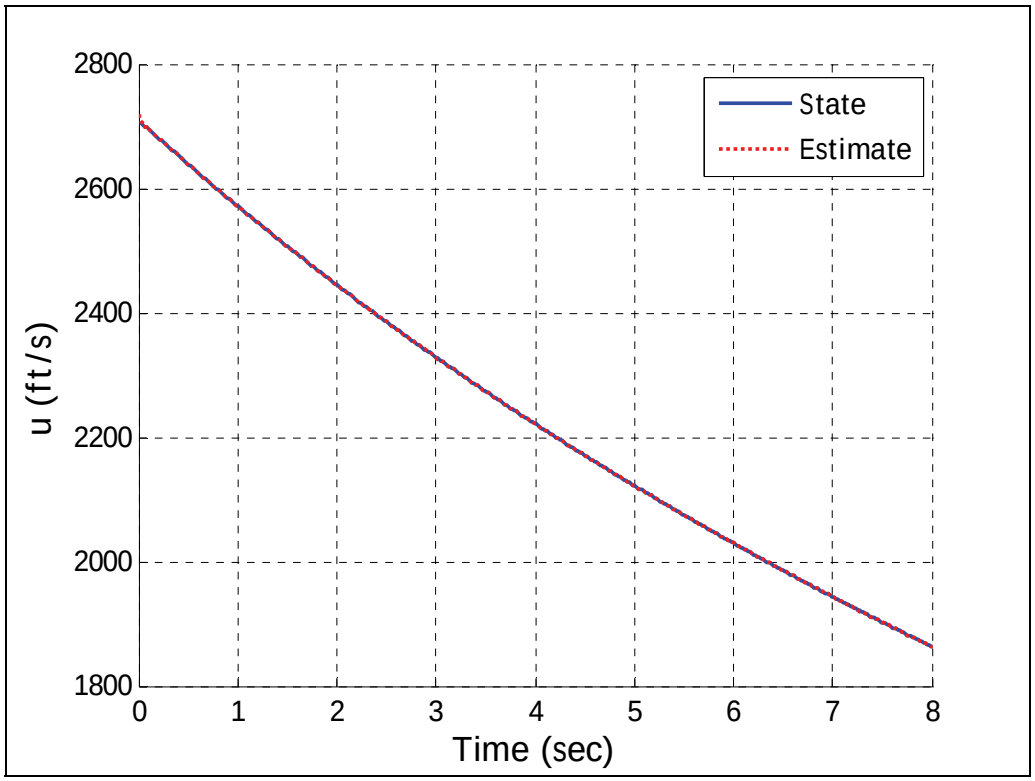

Figure 13. Projectile velocity u.

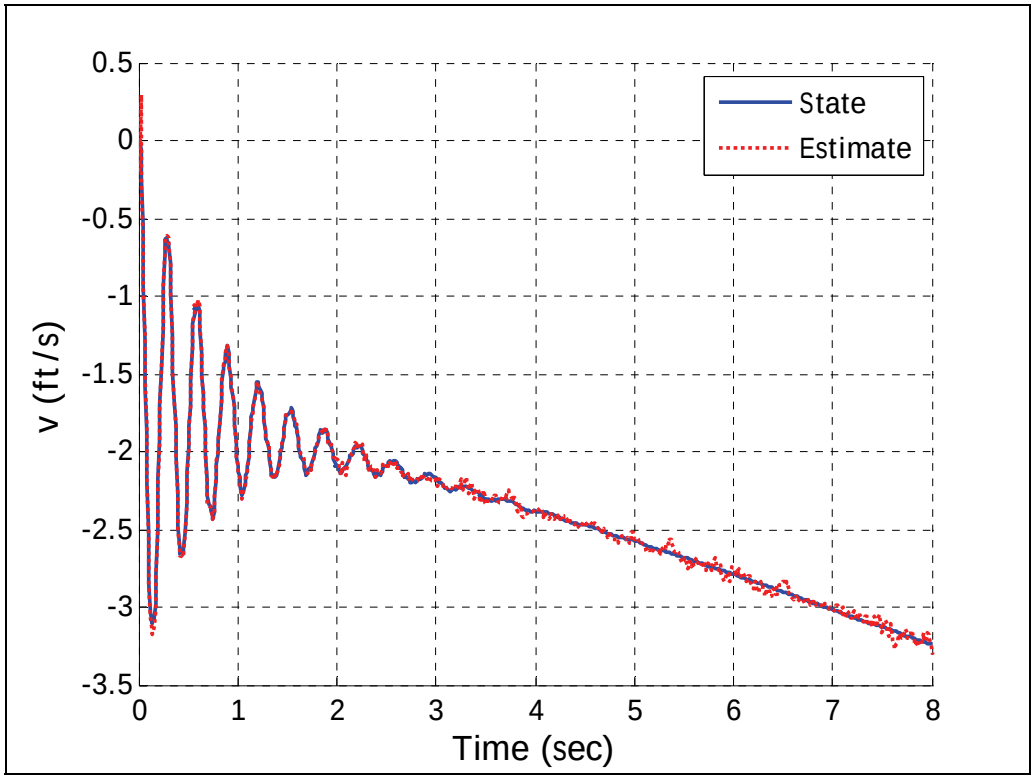

Figure 14. Projectile velocity v.

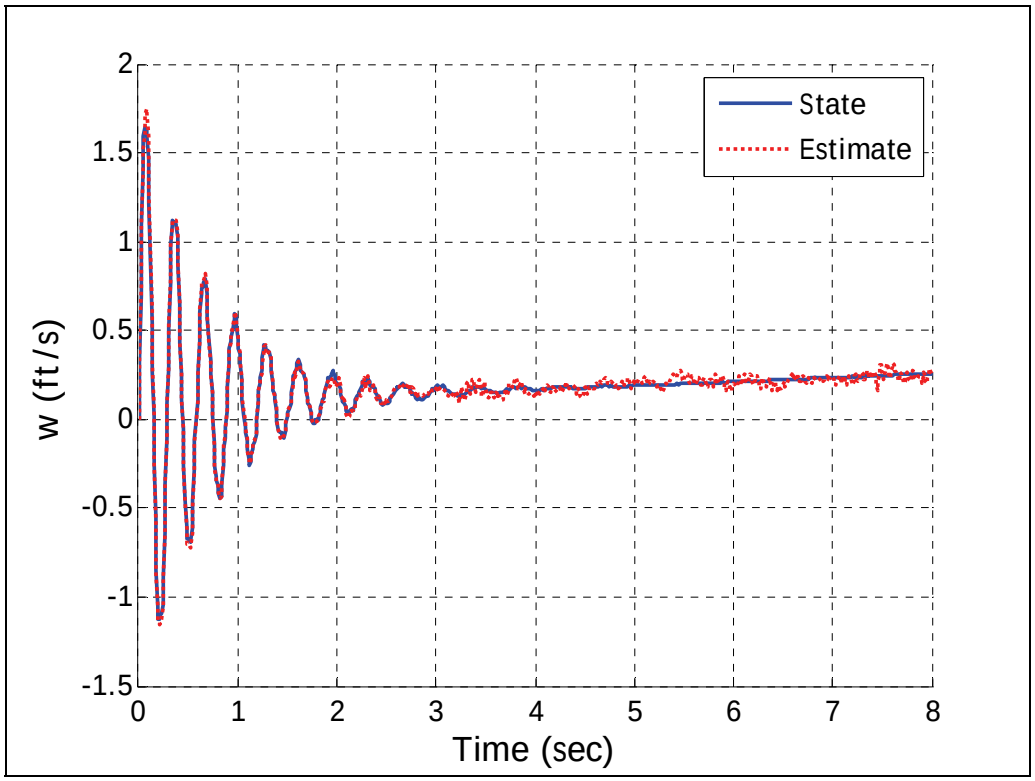

Figure 15. Projectile velocity w.

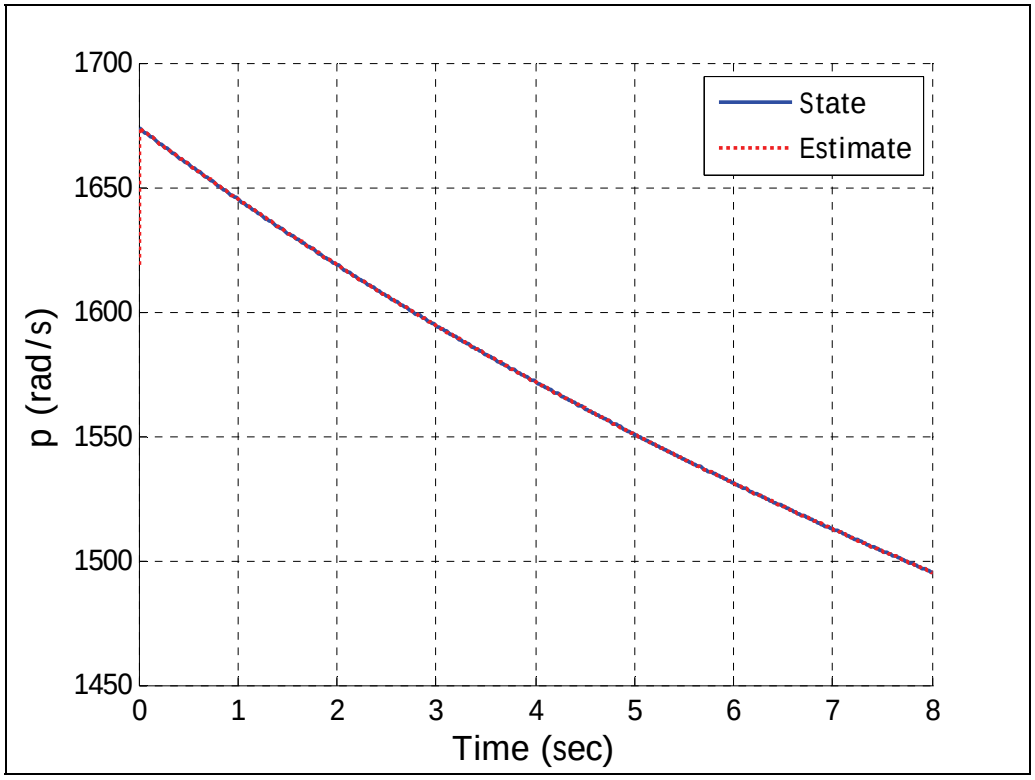

Figure 16. Projectile rate p.

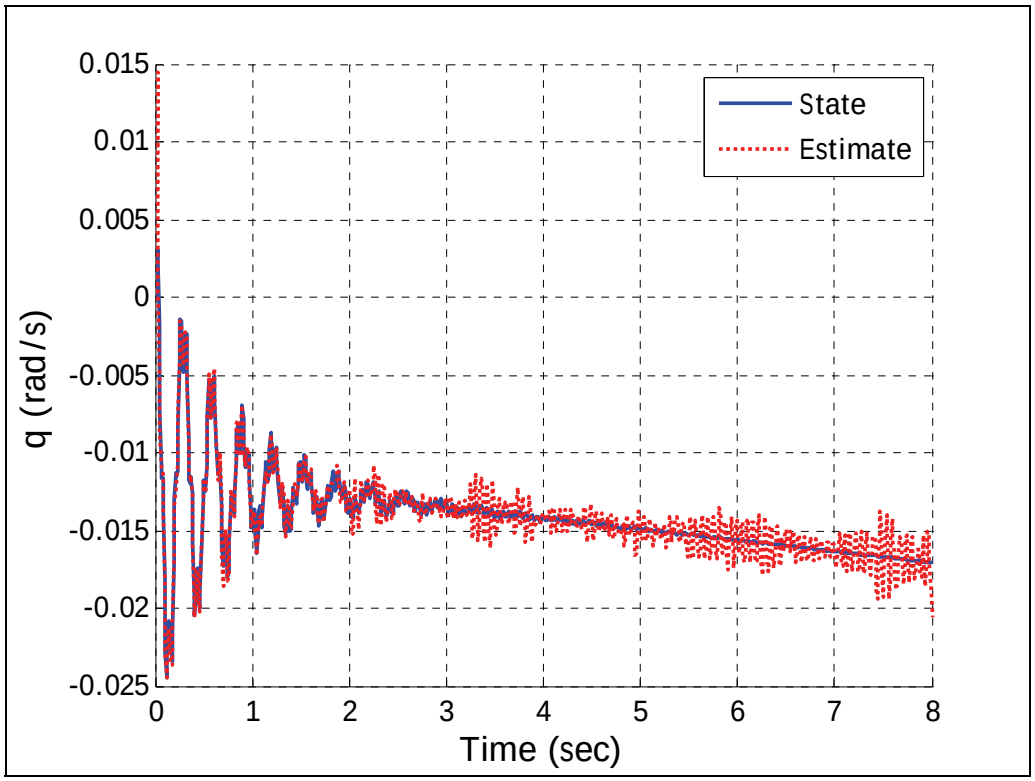

Figure 17. Projectile rate q.

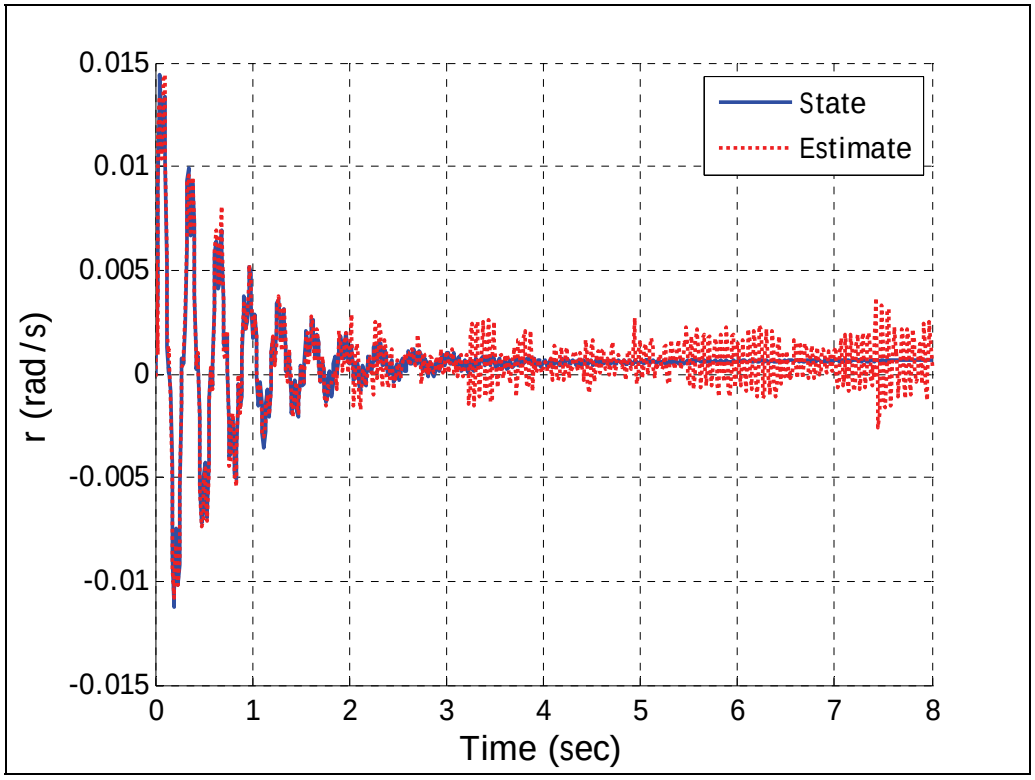

Figure 18. Projectile rate r.

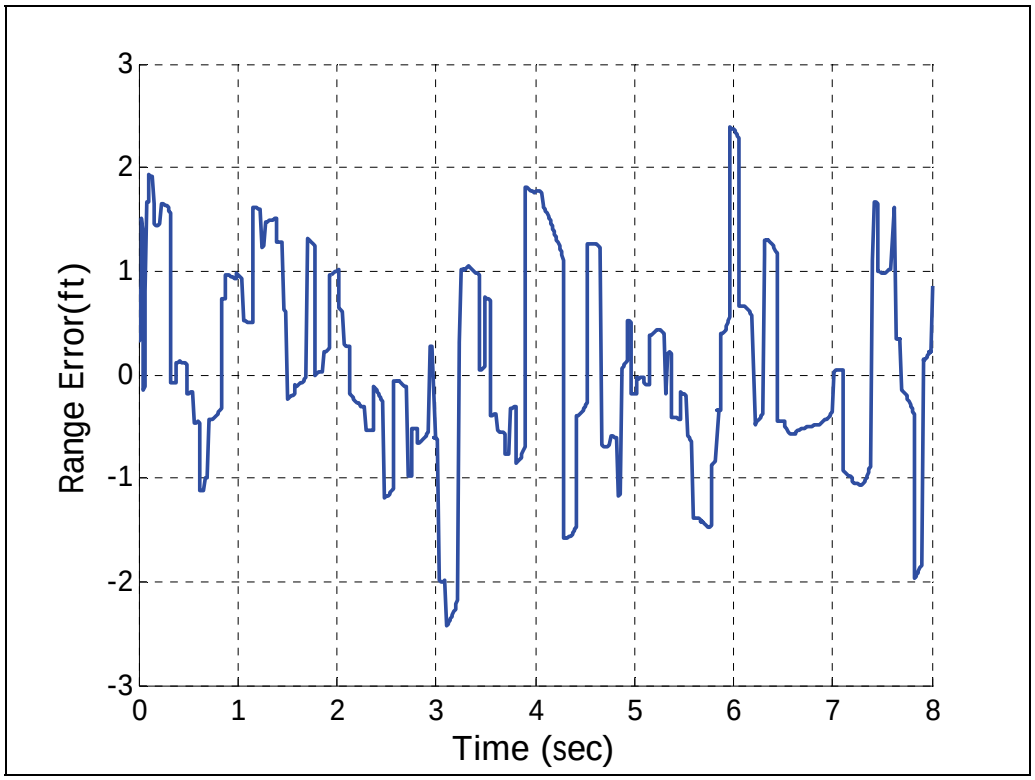

Figure 19. Estimate error in range.

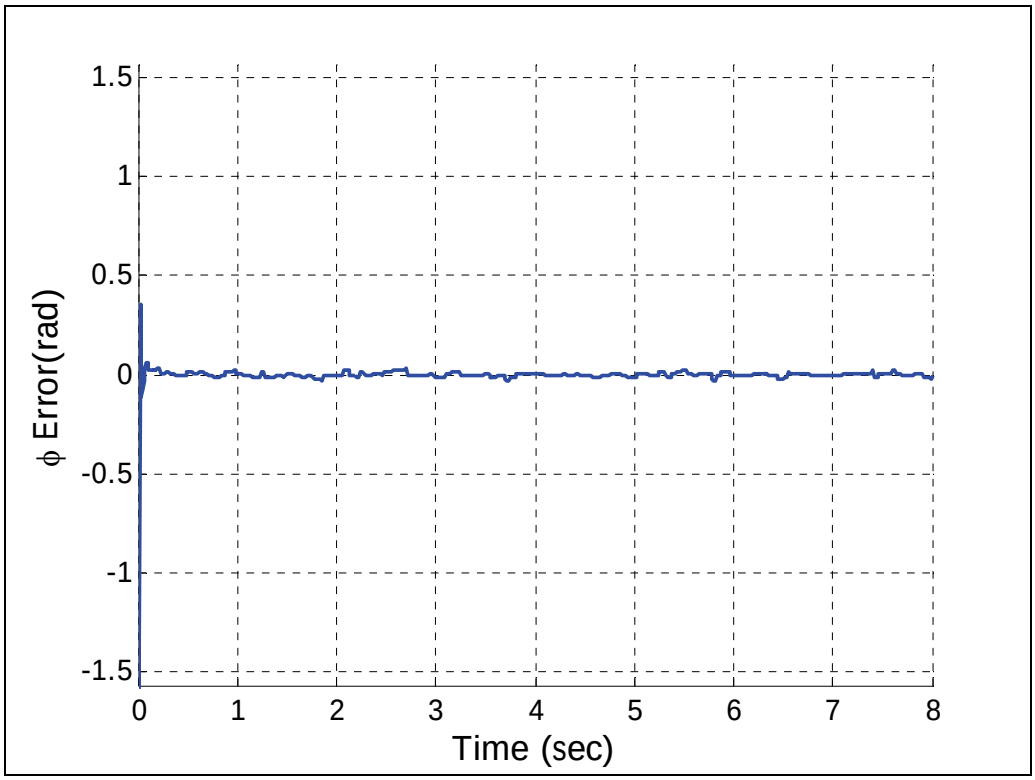

Figure 20. Estimate error in ϕ.

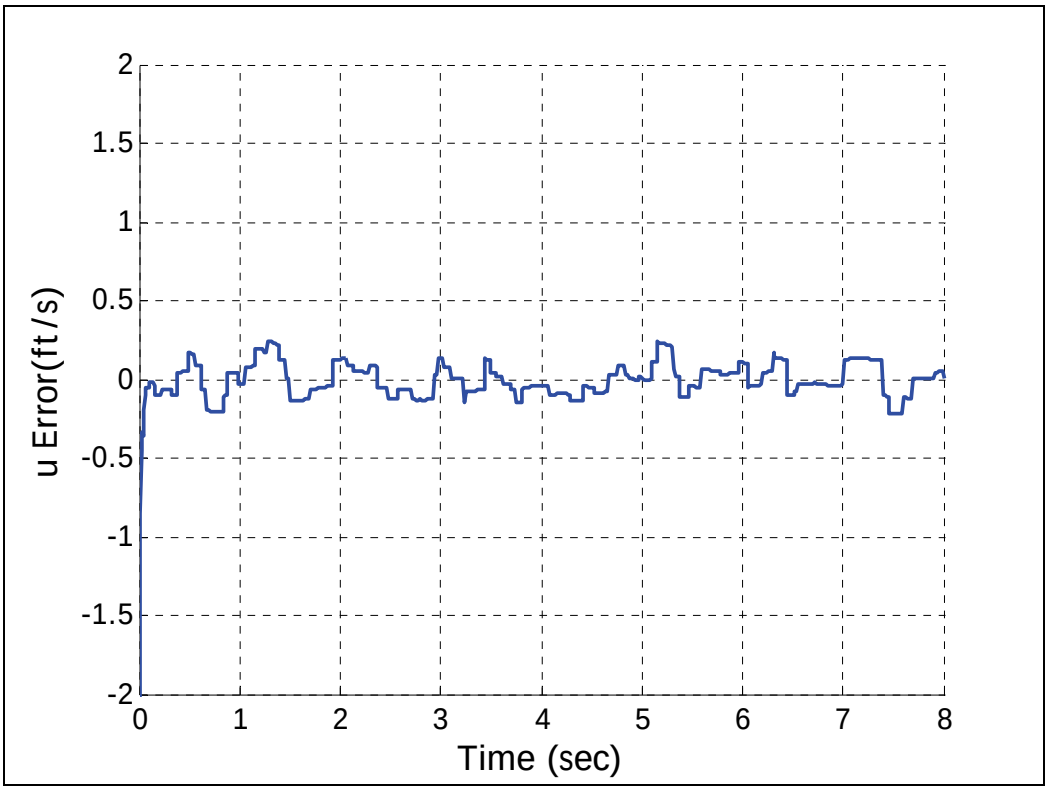

Figure 21. Estimate error in u.

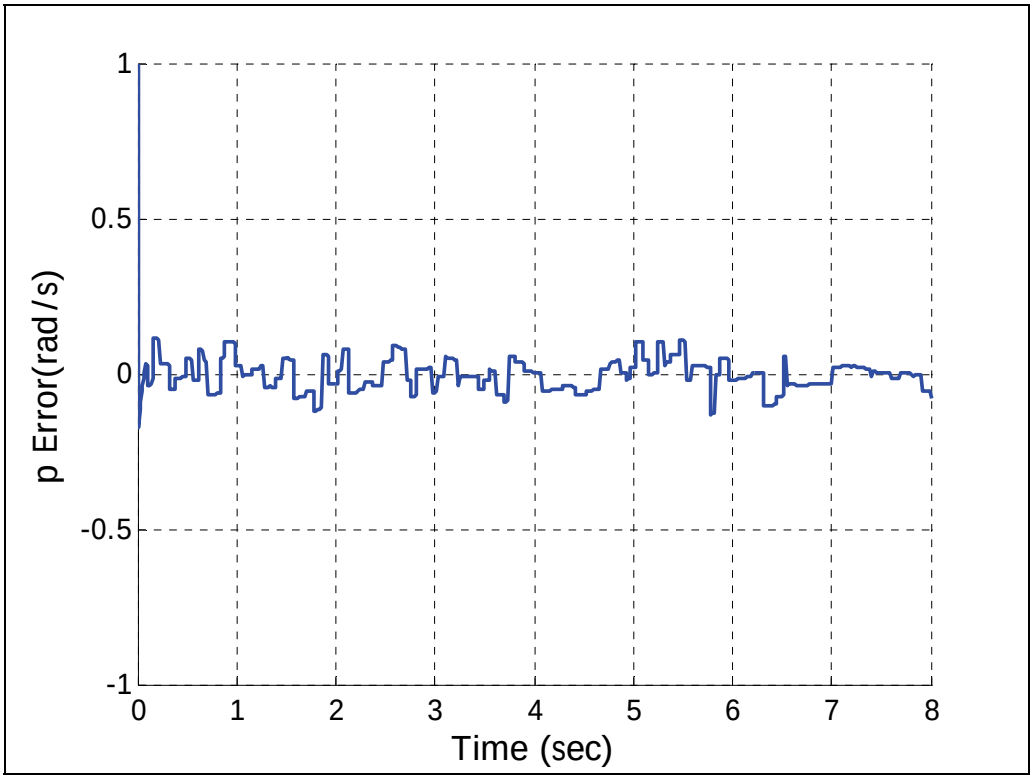

Figure 22. Estimate error in p.

7. References

1. Merhav, S. *Aerospace Sensor Systems and Applications*; Springer-Verlag, Inc.: New York, 1996.

2. Aldrich, G.; Krabill, W. A Versatile Kalman Technique for Aircraft or Missile State Estimation and Error Analysis using Radar Tracking Data. AIAA-72-838, *AIAA Guidance and Control Conference*, Stanford, CA, 1972.

3. Widall, W. Enlarging the Region of Convergence of Kalman Filters that Encounter Nonlinear Elongation of Measured Range. AIAA-72-879, *AIAA Guidance and Control Conference*, Stanford, CA, 1972.

4. Speyer, J.; Hull, D. Comparison of Several Extended Kalman Filter Formulations for Homing Missile Guidance. AIAA-80-1786, *AIAA Guidance and Control Conference*, Danvers, MA, 1980.

5. Chin, H. Distributed Kalman Filter in an Integrated SAHRS/GPS Navigation System. AIAA-85-1878, *AIAA Guidance, Navigation, and Control Conference*, Snowmass, CO, 1985.

6. Lam, Q.; Pal, P.; Welch, R.; Grossman, W. Magnetometer Based Attitude Determination System using a Reduced Kalman Filter. AIAA-96-3629, *AIAA/AAS Astrodynamics Conference*, San Diego, CA, 1996.

7. Burchett, B.; Costello, M. Specialized Kalman Filtering for Guided Projectiles. AIAA-2001-1120, *AIAA Aerospace Sciences Meeting and Exhibit*, Reno, NV, 2001.

8. Shkolnikov, I.; Shtessel, Y.; Zarchan, P.; Lianos, D. Simulation Study of the Homing Interceptor Guidance Loop with Sliding Mode Observers verses Kalman Filter. AIAA-2001-4216, *AIAA Guidance, Navigation, and Control Conference and Exhibit*, Montreal, Canada, 2001.

9. Kalman, R. E. A New Approach to Linear Filtering and Prediction Problems. *Transactions of the ASME-Journal of Basic Engineering* **1960**, *82*, 34-45.

10. Stengel, R. *Optimal Control and Estimations*; Dover Publications, Inc.: New York, 1994.

11. Coleman, N.; Yip, P.; May, R.; Lin, C.; Feng, X.; Yu, T. Estimation and Prediction of Projectile Trajectory, MET Data and Impact Point. AIAA-1998-5538, *AIAA and SAE, 1998 World Aviation Conference*, Anaheim, CA, Sept. 28-30, 1998.

12. Crassidis, J.; Markley, F. Predictive Filtering for Nonlinear Systems. AIAA-1996-3775, *AIAA Guidance, Navigation, and Control Conference*, San Diego, CA, July 29-21, 1996.

13. Moraal, P. E.; Grizzle, J. W. Observer Design for Nonlinear Systems with Discrete-Time Measurements. *IEEE Transactions on Automatic Control* **March 1995**, *40* (3), 395-404.

14. Michalska, H.; Mayne, D. Q. Moving Horizon Observers and Observer-Based Control. *IEEE Transactions on Automatic Control* **June 1995**, *40* (6), 995-1006.

15. Costello, M.; Anderson, D. Effect of Internal Mass Unbalance on the Terminal Accuracy and Stability of a Projectile. AIAA-1996-3447, *AIAA Atmospheric Flight Mechanics Conference*, San Diego, CA, July 29-21, 1996.

16. Press, W.; Teukolsky, S.; Vetterling, W.; Flannery, B. *Numerical Recipes in C*; Cambridge University Press, New York, pp. 681-685, 1992.

Nomenclature

x,y,z	=	Inertial positions of the system mass center.
ϕ,θ,ψ	=	Euler roll, pitch and yaw angles.
$\tilde{u},\tilde{v},\tilde{w}$	=	Velocity components of mass center in a no-roll reference frame.
$\tilde{p},\tilde{q},\tilde{r}$	=	Angular velocity components in a no-roll reference frame.
I	=	Inertia matrix of system.
a_{Bi}	=	Bias of ith accelerometer.
a_{Ni}	=	Noise of ith accelerometer.
a_i	=	Acceleration reading of ith accelerometer.
c_{Ai}^{j}	=	Cross axis sensitivity of ith accelerometer to the jth direction.
c_{Gi}^{j}	=	Cross axis sensitivity of ith gyroscope to the jth direction.
E_i	=	ith component of the Earth's magnetic field.
G_{Bi}	=	Bias of ith GPS.
G_{Ni}	=	Noise of ith GPS.
G_i	=	Reading of ith GPS.
M_{Ni}	=	Noise of ith magnetometer.
M_i	=	Reading of ith magnetometer.
R_S	=	Rotation matrix from body frame to sensor frame.
$\vec{r}_{\oplus\rightarrow Si}$	=	Distance vector from projectile mass center to ith accelerometer.
s_{Ai}	=	Scale factor of ith accelerometer.
s_{Gi}	=	Scale factor of ith gyroscope.
$\vec{\alpha}_{B/I}$	=	Angular acceleration of projectile with respect to the ground.
δ_{Si}^{j}	=	Misposition of ith accelerometer in the jth direction.
$\vec{\omega}_{B/I}$	=	Angular velocity of projectile with respect to the ground.
ω_{Bi}	=	Bias of ith gyroscope.
ω_{Ni}	=	Noise of ith gyroscope.
ω_i	=	Angular velocity reading of ith gyroscope.
C_B	=	Vector component extraction operator for frame B.
S_B	=	Skew symmetric cross product operator for frame B.

NO. OF COPIES ORGANIZATION

1 (PDF ONLY) DEFENSE TECHNICAL INFORMATION CTR
DTIC OCA
8725 JOHN J KINGMAN RD
STE 0944
FORT BELVOIR VA 22060-6218

1 US ARMY RSRCH DEV & ENGRG CMD
SYSTEMS OF SYSTEMS INTEGRATION
AMSRD SS T
6000 6TH ST STE 100
FORT BELVOIR VA 22060-5608

1 DIRECTOR
US ARMY RESEARCH LAB
IMNE ALC IMS
2800 POWDER MILL RD
ADELPHI MD 20783-1197

1 DIRECTOR
US ARMY RESEARCH LAB
AMSRD ARL CI OK TL
2800 POWDER MILL RD
ADELPHI MD 20783-1197

1 DIRECTOR
US ARMY RESEARCH LAB
AMSRD ARL CS OK T
2800 POWDER MILL RD
ADELPHI MD 20783-1197

4 GEORGIA TECH RSCH INST
ATTN J MCMICHAEL K MASSEY
A LOVAS M HEIGES
7220 RICHARDSON ROAD
SMYRNA GA 30080

1 USAMCOM
ATTN AMSAM RD MG J BAUMANN
REDSTONE ARSENAL AL 35898-5000

1 USAMCOM
ATTN AMSRD AMR SG SD B NOURSE
REDSTONE ARSENAL AL 35898-5000

1 AFRL/MNGN
ATTN GREGG ABATE
101 W EGLIN BLVD STE 332
EGLIN AFB FL 32542

1 DR WILLIAM DAMICO
11100 JOHNS HOPKINS RD
APPLIED PHYSICS LABORATORY
LAUREL MD 20723-6099

NO. OF COPIES ORGANIZATION

1 GEORGIA TECH
DANIEL GUGGENHEIM SCHOOL OF
AEROSPACE ENGINEERING
ATTN DR MARK COSTELLO
270 FERST DRIVE
ATLANTA GA 30332-0150

1 US AMRDEC
ATTN AMSAM RD SS AT
R KRETZSCHMAR
BLDG 5400
REDSTONE ARSENAL AL 35898-5000

1 US RDECOM
AMRDEC
ATTN AMSRD AMR SG CT S DUNBAR
BLDG 5400
REDSTONE ARSENAL AL 35898

1 US RDECOM
ATTN AMSRD AMR SG SD J LOCKER
BLDG 5400
REDSTONE ARSENAL AL 35898-5000

4 COMMANDER ARDEC
ATTN AMSRD AAR AEM L D OKKEN
R BRYAN M HORVATH
P BRISLIN
BLDG 65S
PICATINNY ARSENAL NJ 07806-5000

2 COMMANDER ARDEC
ATTN AMSRD AAR AEM M LUCIANO
M PALATHINGAL
BLDG 65S
PICATINNY ARSENAL NJ 07806-5000

2 COMMANDER ARDEC
ATTN AMSRD AAR AEP E CHRIS STOUT
D CARLUCCI
BLDG 94
PICATINNY ARSENAL NJ 07806-5000

1 COMMANDER ARDEC
ATTN AMSRD AAR AEM J G FLEMING
BLDG 65N
PICATINNY ARSENAL NJ 07806-5000

1 COMMANDER ARDEC
ATTN AMSRD AAR AEM D G MOSHIER
BLDG 65N
PICATINNY ARSENAL NJ 07806-5000

NO. OF COPIES ORGANIZATION

1 COMMANDER ARDEC
ATTN AMSRD AAR AIS SA D ERICSON
BLDG 12
PICATINNY ARSENAL NJ 07806-5000

1 PROJECT MANAGER
TANK MAIN ARMAMENT SYS
ATTN SFAE GCSS TMA D GUZIEWICZ
BLDG 354
PICATINNY ARSENAL NJ 07806-5000

1 APM, SMALL & MEDIUM CALIBER
AMMO OPM-MAS
ATTN SFAE GCSS TMA G DEROSA
BLDG 354
PICATINNY ARSENAL NJ 07806-5000

1 COMMANDER
US ARMY TACOM ARDEC
ATTN SFAE GCSS MAS SMC R KOWALSKI
BLDG 354
PICATINNY ARSENAL NJ 07806-5000

3 COMMANDER
US ARMY TACOM ARDEC
ATTN AMSTA AR FSP P P MAGNOTTI
A LICHTENBERG SCALON
BLDG 61S
PICATINNY ARSENAL NJ 07806-5000

1 COMMANDER
US ARMY TACOM ARDEC
ATTN AMSRD AAR A MUSALLI
BLDG 65S
PICATINNY ARSENAL NJ 07806-5000

2 COMMANDER
US ARMY TACOM ARDEC
ATTN AMSRD AAR AEM L G KOLASA
A MOUNA
BLDG 65S
PICATINNY ARSENAL NJ 07806-5000

13 COMMANDER
US ARMY TACOM ARDEC
ATTN AMSRD AAR AEM A G LIVECCHIA
J GRAU G MALEJKO
E VAZQUEZ W TOLEDO L YEE
R TROHANOWSKY S HAN
W KOENIG S CHUNG
C WILSON
BLDG 95
PICATINNY ARSENAL NJ 07806-5000

NO. OF COPIES ORGANIZATION

1 COMMANDER
US ARMY TACOM ADRDEC
ATTN AMSRD AAR AEM L R SAYER
BLDG 65
PICATINNY ARSENAL NJ 07806-5000

1 COMMANDER
US ARMY TACOM ADRDEC
ATTN SFAE AMO MAS LC F CHANG
BLDG 65
PICATINNY ARSENAL NJ 07806-5000

1 COMMANDER
US ARMY TACOM ADRDEC
ATTN AMSTA AR CCH B S PATEL
BLDG 65
PICATINNY ARSENAL NJ 07806-5000

1 COMMANDER
US ARMY TACOM
ATTN SFAE GCSS W AB QT COL J MORAN
WARREN MI 48397-5000

3 COMMANDER
US ARMY TACOM
ATTN SFAE GCSS W LTC S COOPER
J NEFF J FLECK
WARREN MI 48397-5000

1 COMMANDER
US ARMY TACOM
ATTN SFAE CSS TV LTC R GROLLER
WARREN MI 48397-5000

1 DIRECTOR
US ARMY ARMOR CTR
ATTN ATZK TS W MEINSHAUSEN
FT KNOX KY 40121

2 SFSJM-CDL
HQ US ARMY JOINT MUNITIONS CMD
ATTN AMSIO SMT W HARRIS
M RIVERS
1 ROCK ISLAND ARSENAL
ROCK ISLAND IL 61299-6000

2 DIRECTOR
BENET LABORATORIES
ATTN AMSTA AR CCB J VASILAKIS
R HASENBEIN
WATERVLIET NY 12189

NO. OF
COPIES ORGANIZATION

1 DIRECTOR
BENET LABORATORIES
ATTN AMSTA AR CCB RA G PFLEGL
WATERVLIET NY 12189

2 DIRECTOR
MARINE CORPS PROGRAMS DEPT
NAV SURF WARCENDIC CRANE
ATTN M O'MALLEY M STEINHOFF
700 AMMUNITION RD
FALLBROOK CA 92028-3187

ABERDEEN PROVING GROUND

1 DIRECTOR
US ARMY RSCH LABORATORY
ATTN AMSRD ARL CI OK (TECH LIB)
BLDG 4600

32 DIRECTOR
US ARMY RSCH LABORATORY
ATTN AMSRD ARL WM P PLOSTINS (5 CYS)
AMSRD ARL WM B M ZOLTOSKI
J NEWILL
AMSRD ARL WM BA D LYON
T BROWN D HEPNER B DAVIS
G KATULKA
AMSRD ARL WM BC J SAHU
P WEINACHT B GUIDOS (10 CYS)
S SILTON I CELMINS G COOPER
J DESPIRITO J GARNER M BUNDY
B HOWELL
AMSRD ARL WM SG W CIEPIELA